

---

# MODELING ADAGRAD, RMSPROP, AND ADAM WITH INTEGRO-DIFFERENTIAL EQUATIONS

Carlos Heredia\*

carlosherediapimienta@gmail.com

## ABSTRACT

In this paper, we propose a continuous-time formulation for the AdaGrad, RMSProp, and Adam optimization algorithms by modeling them as first-order integro-differential equations. We perform numerical simulations of these equations to demonstrate their validity as accurate approximations of the original algorithms. Our results indicate a strong agreement between the behavior of the continuous-time models and the discrete implementations, thus providing a new perspective on the theoretical understanding of adaptive optimization methods.

## 1 INTRODUCTION

Central to numerous machine learning tasks is the challenge of solving the following optimization problem:

$$\arg \min_{\theta \in \mathbb{R}^n} f(\theta),$$

where  $f : \mathbb{R}^n \rightarrow \mathbb{R}$  denotes a typically non-convex and differentiable objective (or loss) function. The pursuit of finding the global minima of such functions presents a significant challenge due to the inherent complexity and non-convexity of the landscape.

Gradient Descent (GD) remains one of the most prominent algorithms for minimizing the function  $f$  by iteratively finding the optimal parameters  $\theta$  Boyd & Vandenberghe (2004). It operates by adjusting the parameters in the direction of the steepest descent of  $f$  with a fixed step size  $\alpha$  (learning rate). At each iteration, the algorithm computes the gradient of  $f$  with respect to  $\theta$ , guiding the parameter updates to minimize  $f$  progressively Rumelhart et al. (1986):

$$\theta_t \leftarrow \theta_{t-1} - \alpha \nabla_{\theta} f_t(\theta_{t-1}). \quad (1)$$

While Stochastic Gradient Descent (SGD) Bottou (2010) extends the Gradient Descent method by using mini-batches, or randomly selected subsets of data, to compute gradients, this article focuses on a non-stochastic perspective. The continuous nature of these methods permits a more direct application of differential equation techniques. For readers interested in a continuous description of the stochastic method, we refer to Sirignano & Spiliopoulos (2017).

Adaptive optimization methods such as AdaGrad Duchi et al. (2011) and RMSProp Hinton (2012) have been pivotal in advancing gradient-based algorithms. AdaGrad adapts the learning rate for each parameter by accumulating the sum of past squared gradients, which can lead to a significant decrease in the learning rate over time. In contrast, RMSProp mitigates this issue by maintaining an exponentially weighted average of squared gradients, ensuring a more stable learning process. These innovations laid the groundwork for more sophisticated algorithms like Adam.

Adam (Adaptive Moment Estimation) Kingma & Ba (2014) refines gradient descent by computing adaptive learning rates for each parameter, leveraging both the first moment and the second moment of the gradients. Variants like AdamW Loshchilov & Hutter (2017) and AdamL2 have been proposed to address specific issues such as weight decay and improved regularization.

To analyze these optimization algorithms through a continuous framework, we employ well-established tools from differential equations to examine the convergence and stability of these methods. For example, as the learning rate tends to zero ( $\alpha \rightarrow 0$ ), the gradient descent algorithm,

---

\*Independent Researcher, carlosherediapimienta.com

interpreted via the Euler method, can be approximated by the following first-order differential equation:

$$\dot{\theta} = -\nabla_{\theta} f(\theta).$$

Given that the AdaGrad, RMSProp, and Adam algorithms incorporate memory effects through the accumulation of past gradients, they are naturally expected to be represented by integro-differential operators. The primary contributions of this work are summarized as follows:

- We propose continuous formulations for the AdaGrad, RMSProp, and Adam algorithms using integro-differential equations, as described in Propositions 1 to 3. We emphasize that the memory effects are encapsulated within the nonlocal terms of these equations.
- We provide a numerical comparison between the results obtained from these continuous models and the original discrete algorithms, focusing on the accuracy and dynamics of the continuous approximations: Figures 8 to 14. Additionally, we detail the numerical methods employed to solve the integro-differential equations.

This article is organized as follows:

**Sec. 2. Optimization Algorithms.** We review the AdaGrad, RMSProp, and Adam algorithms and present numerical simulations that illustrate their dynamic behavior.

**Sec. 3. Continuous Representations.** We introduce the continuous versions of these algorithms as first-order integro-differential equations.

**Sec. 4. Numerical Simulations.** We compare the numerical results obtained from these continuous models with those from the discrete algorithms, and we provide a detailed explanation of the numerical method used to solve the integro-differential equations.

## 1.1 NOTATION

In this subsection, we introduce and define the notation used throughout the article. Although the notation may appear “highly” physical, it is selected for its simplicity and to enhance the reader’s comprehension.

Our discussion is set within an  $n$ -dimensional Euclidean space, and the key elements of the notation are as follows:

- **Parameter Space:** The parameters  $\theta$  are represented as vectors in  $\mathbb{R}^n$ , where  $\mathbb{R}$  denotes the set of real numbers. These parameters are assumed to be differentiable functions.
- **Euclidean Metric:** The Euclidean metric  $\delta_{ij}$  is employed to raise and lower indices, where  $\delta_{ij}$  is the Kronecker delta.
- **Einstein Summation Convention:** We adopt the Einstein summation convention, wherein repeated indices imply summation over the corresponding index range. For example:

$$\theta^2 := \|\theta\|^2 := \theta_i \theta^i = \delta_{ij} \theta^i \theta^j = \sum_{i=1}^n \theta^i \theta^i,$$

which represents the squared Euclidean norm of the vector  $\theta$ .

- **Derivative Notation:** The partial derivative with respect to the  $i$ -th component of  $\theta$  is denoted by  $\partial_i$ . Specifically, the gradient operator is expressed as:

$$\nabla_{\theta} = \left( \frac{\partial}{\partial \theta^1}, \dots, \frac{\partial}{\partial \theta^i}, \dots, \frac{\partial}{\partial \theta^n} \right) := (\partial_1, \dots, \partial_i, \dots, \partial_n).$$

## 1.2 RELATED WORK

Adaptive optimization algorithms like AdaGrad, RMSProp, and Adam are widely adopted in deep learning due to their robustness and efficiency. However, the inherently discrete nature of deep learning algorithms has led researchers to explore continuous representations to gain deeper theoretical insights and leverage mathematical tools from continuous dynamical systems.

---

**Continuous Representations:** Researchers have extended discrete optimization algorithms to continuous settings using differential equations. For instance, Su et al. (2016) provide a theoretical framework that connects Nesterov’s accelerated gradient method with a second-order ordinary differential equation (ODE), offering insights into the convergence properties and dynamics of optimization algorithms. Similarly, Wibisono et al. (2016) present a variational perspective on accelerated methods by deriving ODEs using a Lagrangian framework, capturing the essence of momentum in optimization.

These continuous formulations allow for the analysis of optimization dynamics and convergence properties, such as asymptotic Lyapunov stability Gantmakher (1970). Stability analysis helps determine whether the solutions of optimization algorithms remain near an equilibrium point or diverge over time, providing deeper insights into their robustness Khalil (2002). Additionally, Romero et al. (2022) focus on the challenge of discretizing continuous-time analogues of optimization algorithms, particularly gradient-based methods, while retaining the optimality properties inherent in the continuous formulation.

Extending this continuous perspective to neural networks, Chen et al. (2018) introduce Neural Ordinary Differential Equations (Neural ODEs), which model the evolution of hidden states in continuous time, bridging the gap between discrete neural networks and continuous dynamical systems. Similarly, Ruthotto & Haber (2020) explore how partial differential equations (PDEs) can be used to model and design deep neural networks. By interpreting layers in a neural network as time steps in a PDE solver, they provide a continuous-time perspective that can lead to new architectures and training algorithms, such as parabolic, elliptic, and hyperbolic CNNs.

On another front, Li et al. (2017) explore stochastic gradient algorithms through stochastic differential equations (SDEs), providing a deeper understanding of their behavior in the continuous limit. This perspective is valuable for analyzing the convergence and stability properties of stochastic optimization methods.

**Integro-Differential Equations and Memory Effects:** Recent research has examined the use of integro-differential equations (IDEs) to model biological and physical processes, as they can more accurately capture memory and cumulative effects than ODEs. For instance, Zappala et al. (2022) introduce Neural Integro-Differential Equations, combining neural networks with IDEs to model systems where both past and future states influence the current state. This approach is particularly effective in extrapolating temporal data and generalizing to unseen initial conditions, providing a framework for modeling complex dynamics with nonlocal interactions.

**Physical Perspectives on Optimization:** Weinan E (2017) suggests rethinking machine learning algorithms through the lens of dynamical systems and control theory. In this view, optimization algorithms are modeled as continuous-time dynamical systems, treating learning as a control problem where parameters are adjusted for optimal outcomes. He also proposes that this continuous framework makes it possible to apply advanced control techniques, such as adaptive time-stepping, Hamiltonian structures, and constraints, to improve the efficiency and stability of machine learning models.

In this context, departing from traditional neural networks that focus on learning mappings between inputs and outputs, Hamiltonian Neural Networks (HNNs) Greydanus et al. (2019) and Lagrangian Neural Networks (LNNs) Cranmer et al. (2020) incorporate fundamental physical principles directly into their architectures. HNNs are rooted in Hamiltonian mechanics and are trained to learn a Hamiltonian function that inherently respects exact conservation laws in an unsupervised manner. This approach makes them particularly effective for modeling systems where energy conservation is critical, such as the two-body problem. Conversely, LNNs employ the Euler-Lagrange equations by parameterizing arbitrary Lagrangian functions using neural networks without requiring canonical coordinates. This capability enables LNNs to perform well in situations where canonical momenta are unknown or difficult to compute.

Noether’s theorem, which establishes a fundamental connection between symmetries and conserved quantities in physical systems, has also inspired advancements in machine learning. For example, Noether Networks Alet et al. (2021) leverage this theorem to meta-learn conserved quantities, improving prediction quality in sequential problems. Furthermore, Tanaka & Kunin (2021) develop a theoretical framework to study the geometry of learning dynamics in neural networks, revealing a

---

key mechanism of explicit symmetry breaking behind the efficiency and stability of modern neural networks.

While previous works have successfully employed ordinary differential equations (ODEs) and partial differential equations (PDEs) to model optimization algorithms and neural networks, they often focus on methods without explicit memory terms or cumulative effects. Our work distinguishes itself by proposing continuous formulations of AdaGrad, RMSProp, and Adam using integro-differential equations. By explicitly modeling the memory effects inherent in these adaptive algorithms through integral operators, we provide a novel perspective that captures their nonlocal dynamics. This distinction is crucial for achieving a deeper theoretical understanding and for developing new optimization strategies inspired by nonlocal behaviors, setting our work apart from prior studies that model optimization algorithms solely as ODEs.

Therefore, our approach allows us to: (a) accurately represent cumulative effects by directly modeling how past gradients influence current updates—a defining characteristic of adaptive optimization algorithms; (b) facilitate theoretical analysis, as the continuous framework enables the application of advanced mathematical tools from the theory of integro-differential equations, such as stability analysis and convergence proofs; and (c) bridge discrete and continuous dynamics, offering insights into the behavior of these algorithms and potential improvements.

## 2 OPTIMIZATION ALGORITHM

In this section, we present the optimization algorithms<sup>1</sup>: AdaGrad, RMSProp, and Adam, with the aim of illustrating the evolution of the parameters as they converge towards the minimum of the function:

$$f(\theta) = (\theta - 4)^2.$$

This function is chosen for its convexity and differentiability, with a known minimum at  $\theta = 4$ . The simplicity of this function allows for straightforward analytical determination of the minimum, facilitating direct comparisons with numerical simulations. For an additional example involving the Mean Squared Error (MSE) loss function, refer to the appendix B.

### 2.1 FUNDAMENTALS OF ADAGRAD

The Adaptive Gradient Algorithm (AdaGrad), introduced by Duchi et al. (2011), marks a significant advancement in the development of optimization techniques. The primary innovation of AdaGrad is its ability to adapt the learning rate for each parameter individually, based on the historical gradients observed during training.

AdaGrad is distinguished by maintaining a cumulative sum of the squares of past gradients for each parameter, denoted as  $G_k$ . This accumulation effectively scales the learning rate inversely proportional to the square root of  $G_k$ , ensuring that parameters frequently updated receive smaller updates, while parameters updated less frequently receive larger updates.

A notable strength of AdaGrad is its capability to handle scenarios involving sparse features, as it allows for larger updates for parameters associated with infrequent features. However, a limitation arises when the accumulated gradient sum  $G_k$  increases excessively over time, causing the effective learning rate to diminish and potentially leading to premature convergence or slower learning. As will be discussed, this issue is mitigated by the RMSProp algorithm.

#### 2.1.1 MATHEMATICAL FORMULATION OF ADAGRAD AND NUMERICAL SIMULATIONS

Consider an objective function  $f : \mathbb{R}^n \rightarrow \mathbb{R}$ , parameterized by  $\theta \in \mathbb{R}^n$ , with a learning rate  $\alpha \in (0, 1]$ . AdaGrad iteratively updates the parameters as described in Algorithm 1, where  $\epsilon$  is a small constant added to prevent division by zero (typically  $\sim 10^{-8}$ ), and  $k$  denotes the current timestep.

---

<sup>1</sup>For a comprehensive overview of Gradient Descent optimization algorithms, see Ruder (2016).

---

**Algorithm 1** AdaGrad Optimization Algorithm

---

- 1: Initialize parameters  $\theta_{k=0}^i$  and the accumulated squared gradient sum  $G_{k=0} = 0$ .
  - 2: **while** the parameters  $\theta_k^i$  have not converged **do**
  - 3:      $k \leftarrow k + 1$
  - 4:     Compute the gradient:  $g_k^i \leftarrow \delta^{ij} \partial_j f(\theta_{k-1})$ .
  - 5:     Accumulate gradients:  $G_k \leftarrow G_{k-1} + g_k^2$
  - 6:     Update parameters:  $\theta_k^i \leftarrow \theta_{k-1}^i - \alpha g_k^i / (\sqrt{G_k} + \epsilon)$
  - 7: **end while**
- 

**Numerical Simulation:** Figure 1 illustrates the convergence trajectories of  $\theta$  as the AdaGrad algorithm minimizes the function  $f(\theta) = (\theta - 4)^2$ , using two different learning rates ( $\alpha = 0.1$  and  $\alpha = 0.01$ ). For  $\alpha = 0.1$ ,  $\theta$  converges towards the minimum value of 4 within fewer than 2000 iterations. The curve flattens as the algorithm stabilizes at the minimum. Conversely, with a smaller learning rate of  $\alpha = 0.01$ , convergence is significantly slower, taking over 150,000 iterations to reach the same minimum. This is due to the convex nature of the function, where larger steps allow the algorithm to reach the minimum more quickly compared to smaller steps.

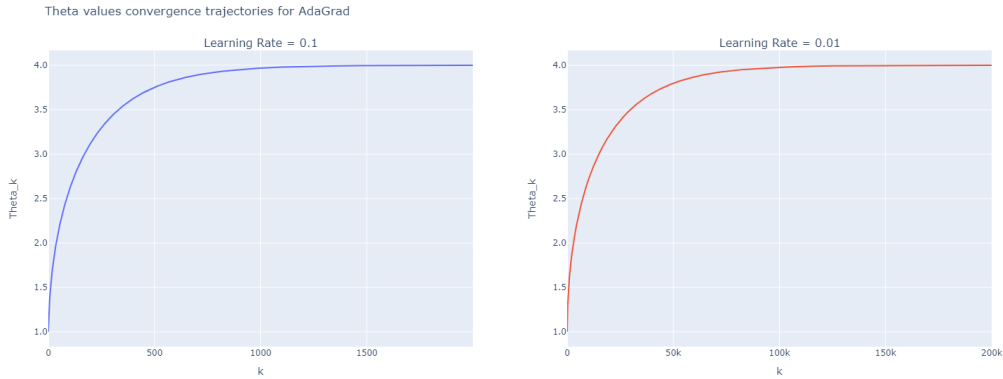


Figure 1: **Trajectory of the Discrete AdaGrad Algorithm.** The plot shows the convergence of  $\theta$  towards the minimum of the function for two learning rates ( $\alpha = 0.1$  and  $\alpha = 0.01$ ). In both cases,  $\theta$  converges to 4, the minimum of the function  $f(\theta) = (\theta - 4)^2$ .

Figure 2 shows the accumulation of squared gradients  $G_k$  over the iterations for the same learning rates. With  $\alpha = 0.1$ , the accumulation of gradients stabilizes relatively quickly, corresponding to the fast convergence observed in Figure 1. For  $\alpha = 0.01$ , however, the accumulation grows more gradually, reflecting the slower convergence of  $\theta$ .

## 2.2 FUNDAMENTALS OF RMSPROP

The Root Mean Square Propagation (RMSProp) optimizer, introduced by Hinton in his lecture series Hinton (2012), was developed primarily to address the issue of diminishing learning rates encountered in AdaGrad, which can slow down convergence over time.

RMSProp distinguishes itself by maintaining a moving average of the squared gradients for each parameter, denoted as  $v$ . This method allows the algorithm to adaptively adjust the learning rate based on the recent magnitude of the gradients, effectively preventing the learning rate from becoming excessively small. The moving average is computed using an exponential decay rate  $\beta$ , which determines the influence of recent gradients on the current value of  $v$ . A  $\beta$  value close to 1 reduces the impact of recent gradients, resulting in a smoother and more stable average.

A key advantage of RMSProp is its ability to maintain a more consistent learning rate throughout the optimization process. By avoiding the drastic reduction in learning rates seen in AdaGrad, RMSProp allows for more sustained and effective learning over time.

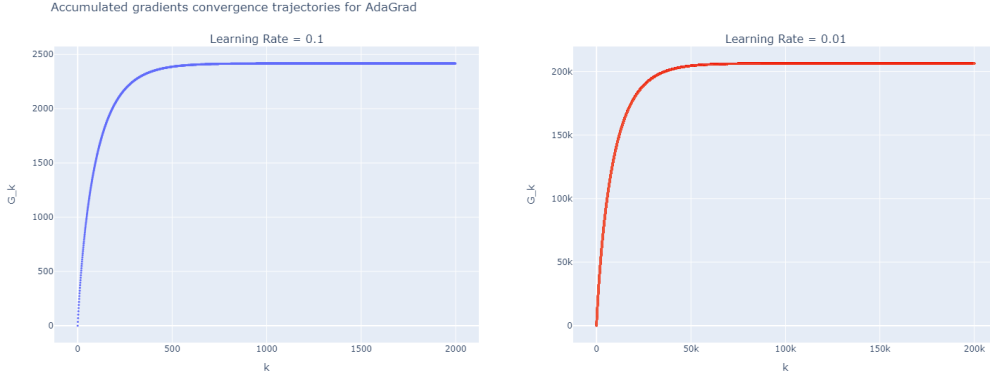


Figure 2: **Trajectory of the Accumulated Gradient for the AdaGrad Algorithm.** The plot tracks the value of  $G_k$  as it is iteratively updated by the AdaGrad optimizer to converge towards the minimum of the function  $f(\theta) = (\theta - 4)^2$ .

### 2.2.1 MATHEMATICAL FORMULATION OF RMSPROP AND NUMERICAL SIMULATIONS

Consider an objective function  $f : \mathbb{R}^n \rightarrow \mathbb{R}$ , parameterized by  $\theta \in \mathbb{R}^n$ , and an exponential decay rate  $\beta \in [0, 1)$ . RMSProp iteratively updates the parameters as described in Algorithm 2, where  $\alpha \in (0, 1]$  denotes the learning rate,  $\epsilon$  is a small constant to prevent division by zero (typically  $\sim 10^{-8}$ ), and  $k$  is the current timestep.

---

#### Algorithm 2 RMSProp Optimization Algorithm

---

- 1: Initialize parameters  $\theta_{k=0}^i$  and the squared gradient moving average  $v_{k=0} = 0$ .
  - 2: **while** the parameters  $\theta_k^i$  have not converged **do**
  - 3:      $k \leftarrow k + 1$
  - 4:     Compute the gradient:  $g_k^i \leftarrow \delta^{ij} \partial_j f(\theta_{k-1})$ .
  - 5:     Update the squared gradient moving average:  $v_k \leftarrow \beta v_{k-1} + (1 - \beta) g_k^2$
  - 6:     Update parameters:  $\theta_k^i \leftarrow \theta_{k-1}^i - \alpha g_k^i / (\sqrt{v_k} + \epsilon)$
  - 7: **end while**
- 

**Numerical Simulations:** Figure 3 illustrates the convergence trajectories of  $\theta$  for different values of  $\beta \in \{0.0, 0.9, 0.99\}$  and learning rates ( $\alpha = 0.1$  and  $\alpha = 0.01$ ). With a higher learning rate of  $\alpha = 0.1$ , RMSProp exhibits varied behavior depending on the value of  $\beta$ :

For  $\beta = 0.0$ , the algorithm converges quickly but shows significant oscillations near the minimum, indicating a high sensitivity to recent gradients and leading to unstable updates. As  $\beta$  increases to 0.9 and 0.99, the oscillations diminish, resulting in smoother convergence. Furthermore, with  $\beta = 0.99$ , the convergence speed improves, demonstrating a positive correlation between stability and convergence rate.

When the learning rate is reduced to  $\alpha = 0.01$ , the overall convergence is slower but remains stable across all values of  $\beta$ . Higher values of  $\beta$  continue to offer a smoother trajectory toward the minimum.

Figure 4 compares the behavior of the squared gradients  $v_k$  for different values of  $\beta \in \{0.0, 0.9, 0.99\}$ . In RMSProp, the squared gradients tend to saturate at 0.0, a behavior that contrasts with AdaGrad, where the squared gradients stabilize at non-zero values.

With  $\alpha = 0.1$ , RMSProp demonstrates that the squared gradients  $v_k$  decrease rapidly when  $\beta = 0.0$ , often leading to saturation at 0.0. As  $\beta$  increases, the decrease in  $v_k$  becomes more gradual, reducing the likelihood of immediate saturation. At a lower learning rate of  $\alpha = 0.01$ , the squared gradients in RMSProp decrease more slowly, particularly with higher values of  $\beta$ , where the initial bump becomes more pronounced but ultimately still declines to 0.

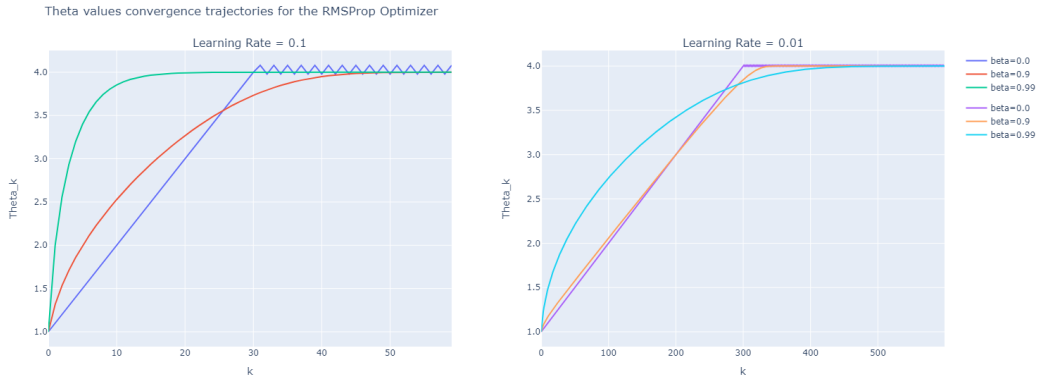


Figure 3: **Trajectory of the Discrete RMSProp Algorithm.** The plot illustrates the convergence trajectories of  $\theta$  for different values of  $\beta \in \{0.0, 0.9, 0.99\}$  across two learning rates ( $\alpha = 0.1$  and  $\alpha = 0.01$ ). In all cases,  $\theta$  converges towards the minimum value of 4, corresponding to the minimum of the function  $f(\theta) = (\theta - 4)^2$ . Compared to AdaGrad, RMSProp converges faster, but oscillations can occur when  $\beta$  is set to or close to 0. These oscillations diminish as  $\beta$  increases, resulting in smoother convergence.

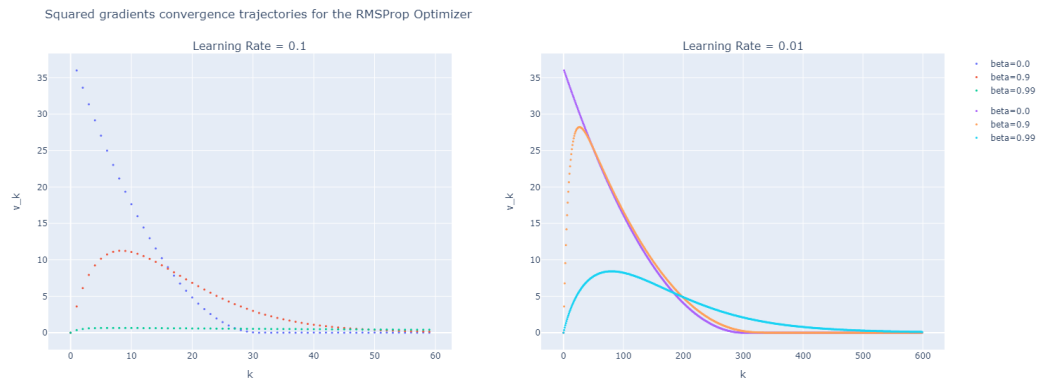


Figure 4: **Trajectory of the Accumulated Gradient for the RMSProp Algorithm.** The plot tracks the convergence of the accumulated squared gradients  $v_k$  for the same  $\beta$  and  $\alpha$  configurations shown in Figure 3. In all cases, the squared gradients  $v_k$  decrease over time as the optimizer progresses. Unlike AdaGrad, where squared gradients stabilize at non-zero values, RMSProp tends to saturate at 0.0 as the learning rate decreases. Depending on the value of  $\beta$ , the squared gradients either decay directly to 0 or exhibit an initial bump that quickly falls to 0.

### 2.3 FUNDAMENTALS OF ADAM

The Adaptive Moment Estimation (Adam) optimizer, introduced by Kingma and Ba (2014) Kingma & Ba (2014), represents also a significant advancement in optimization techniques, particularly in the fields of deep learning. It combines the strengths of two other gradient-based optimization methods: the Adaptive Gradient Algorithm and Root Mean Square Propagation.

Adam distinguishes itself by maintaining two separate moving averages for each parameter: the first moment,  $m^i$ , and the second moment,  $v$ . The first moment estimates the gradients, while the second moment estimates the squared gradients, similar to RMSProp’s adaptive learning rates. These moving averages are computed using exponential decay rates,  $\beta_1$  and  $\beta_2$ , respectively.

Values of  $\beta_1$  and  $\beta_2$  close to 1 imply a longer memory of past gradients, effectively smoothing the averages over a larger number of iterations. This smoothing helps stabilize the optimization process by reducing the impact of sudden changes in gradient values.

### 2.3.1 MATHEMATICAL FORMULATION OF ADAM AND NUMERICAL SIMULATIONS

Consider an objective function  $f : \mathbb{R}^n \rightarrow \mathbb{R}$ , parameterized by  $\theta \in \mathbb{R}^n$ , with exponential decay rates  $\beta_1, \beta_2 \in [0, 1)$ . Adam iteratively updates the parameters as described in Algorithm 3, where  $\alpha \in (0, 1]$  denotes the learning rate,  $\epsilon$  is a small constant to prevent division by zero (typically  $\sim 10^{-8}$ ), and  $k$  is the current timestep.

---

#### Algorithm 3 Adam Optimization Algorithm

---

- 1: Initialize the parameters  $\theta_{k=0}^i$ , the first moment  $m_{k=0}^i = 0$ , and the second moment  $v_{k=0}^i = 0$ .
  - 2: **while** the parameters  $\theta_k^i$  have not converged **do**
  - 3:    $k \leftarrow k + 1$
  - 4:   Compute the gradient:  $g_k^i \leftarrow \delta^{ij} \partial_j f(\theta_{k-1})$ .
  - 5:   Update first moment:  $m_k^i \leftarrow \beta_1 m_{k-1}^i + (1 - \beta_1) g_k^i$
  - 6:   Update second moment:  $v_k \leftarrow \beta_2 v_{k-1} + (1 - \beta_2) g_k^2$
  - 7:   Correct first moment:  $\hat{m}_k^i \leftarrow m_k^i / (1 - \beta_1^k)$
  - 8:   Correct second moment:  $\hat{v}_k \leftarrow v_k / (1 - \beta_2^k)$
  - 9:   Update parameters:  $\theta_k^i \leftarrow \theta_{k-1}^i - \alpha \hat{m}_k^i / (\sqrt{\hat{v}_k} + \epsilon)$
  - 10: **end while**
- 

**Numerical Simulations:** Figure 5 illustrates the convergence of  $\theta$  to the minimum,  $\theta = 4$ , of the objective function  $f(\theta) = (\theta - 4)^2$  using the Adam optimizer, under different configurations<sup>2</sup> of  $\beta_1 \in \{0.0, 0.9\}$  and  $\beta_2 \in \{0.99, 0.999\}$ . With a learning rate of  $\alpha = 0.1$ ,  $\theta$  converges rapidly to the minimum, particularly when both  $\beta_1$  and  $\beta_2$  are high (0.9 and 0.99). However, small oscillations around the minimum are observed when  $\beta_1 = 0.9$ , indicating slight instability in convergence. As  $\beta_1$  decreases, these oscillations diminish, allowing for smoother and more stable convergence to the minimum value. At a lower learning rate of  $\alpha = 0.01$ ,  $\theta$  converges more slowly but steadily towards the minimum. Configurations with high  $\beta_1$  and  $\beta_2$  show more controlled convergence, with no oscillations. Compared to AdaGrad and RMSProp, Adam offers a balanced approach: it converges faster than AdaGrad but is slightly slower than RMSProp. Both Adam and AdaGrad or RMSProp share the characteristic that, as the learning rate decreases, convergence to the minimum takes longer, as discussed earlier.

Figure 6 illustrates the convergence trajectories of the first moment  $m_k^i$  for the Adam optimizer, considering different values of  $\beta_1$  and  $\beta_2$ , under two learning rates ( $\alpha = 0.1$  and  $\alpha = 0.01$ ). With a learning rate of  $\alpha = 0.1$ , it is evident that  $m_k$  exhibits significant initial oscillations, particularly when  $\beta_1 = 0.9$ . As  $\beta_1$  decreases to 0.0, these oscillations diminish, resulting in smoother updates to the moving averages. Regardless of the values of  $\beta_1$ , the moment  $m_k^i$  stabilizes around the same iteration. In contrast, at a lower learning rate of  $\alpha = 0.01$ , the oscillations in  $m_k$  disappear, leading to a more stable convergence. In all cases,  $m_k$  stabilizes around 0.

Figure 7 presents the convergence trajectories of the second moment  $v_k$  under the Adam optimizer, across different configurations of  $\beta_1$ ,  $\beta_2$ , and  $\alpha$ . With a learning rate of  $\alpha = 0.1$ ,  $v_k$  shows significant initial variation, especially when  $\beta_2 = 0.99$ . Here,  $v_k$  increases rapidly and then decreases as the algorithm progresses. When  $\alpha = 0.01$ , a similar dynamic is observed, but the peak is more pronounced for  $\beta_2 = 0.99$ , while for  $\beta_2 = 0.999$ , it rises slightly higher. The initial behavior of  $v_k$  in Adam resembles that of RMSProp, with an initial peak followed by a smooth decline. However, not all configurations stabilize at 0.0 when the minimum is reached.

## 3 TIME-CONTINUOUS MODELS FOR ADA GRAD, RMSPROP AND ADAM

Expressing the optimizers discussed in the previous section within a continuous framework offers several advantages, particularly by enhancing the understanding and analysis of their temporal be-

<sup>2</sup>The motivation for choosing this configuration of  $\beta$  is given by the article Kingma & Ba (2014).



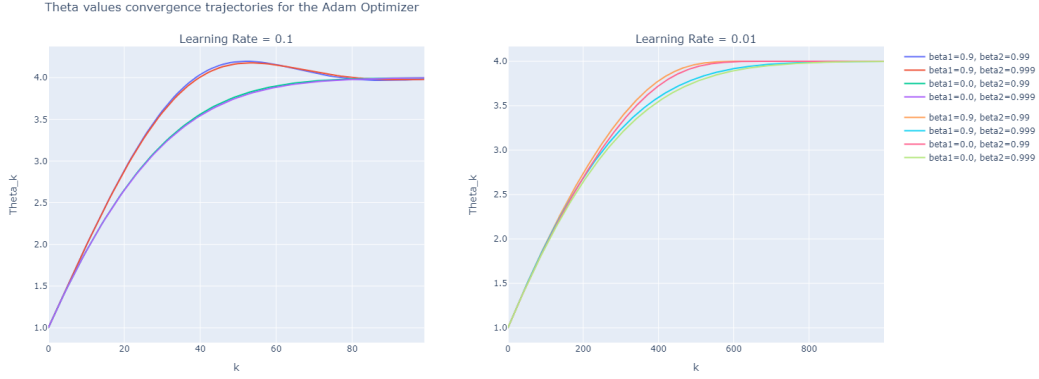


Figure 5: **Trajectory of the Discrete Adam Algorithm.** The plot shows how  $\theta$  converges to the minimum ( $\theta = 4$ ) of the objective function  $f(\theta) = (\theta - 4)^2$  using the Adam optimizer under different configurations of  $\beta_1$  and  $\beta_2$ . Higher values of  $\beta_1$  and  $\beta_2$  generally result in fewer oscillations around the minimum. These oscillations tend to disappear as the learning rate decreases.

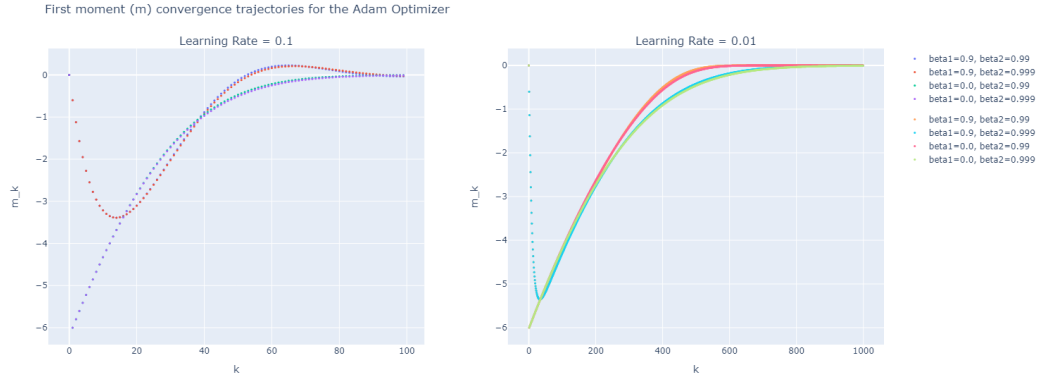


Figure 6: **Trajectory of the First Moment for Adam Algorithm.** The convergence trajectories of the first moment  $m_k$  for different values of  $\beta_1$  and  $\beta_2$  at two learning rates ( $\alpha = 0.1$  and  $\alpha = 0.01$ ). Higher learning rates ( $\alpha = 0.1$ ) show more pronounced oscillations, especially when  $\beta_1$  is high, which diminish as  $\beta_1$  decreases. Lower learning rates ( $\alpha = 0.01$ ) result in more stable trajectories.

havior. Continuous formulations allow the application of advanced mathematical tools, such as Lyapunov stability analysis, to investigate the dynamics of parameter updates and the convergence properties of the algorithm Kovachki & Stuart (2021).

Next, we present three propositions (three continuous-time models) for the optimization algorithms AdaGrad, RMSProp, and Adam. In all cases, we assume the following conditions:

**Assumption 1.** *The relationship between the temporal variable  $t$  and the iteration  $k$  is governed by the learning rate  $\alpha$  such that*

$$t = \alpha k. \tag{2}$$

Building on this assumption,

**Assumption 2.** *Given a small learning rate  $\alpha$ , the timescale relationship is expressed as:*

$$z_{\frac{t+\alpha}{\alpha}}^i := z^i(t + \alpha) \sim z^i(t) + \alpha \dot{z}^i(t) + \mathcal{O}(\alpha^2) \quad \text{and} \quad z_{\frac{t}{\alpha}}^i := z^i(t) \quad \text{for} \quad t > 0.$$

Therefore,

**Proposition 1 (Nonlocal Continuous Dynamics of AdaGrad).** *Under Assumption (2) and with an initial value for the accumulated gradients  $G_0 = 0$ , the continuous nonlocal dynamics of AdaGrad*

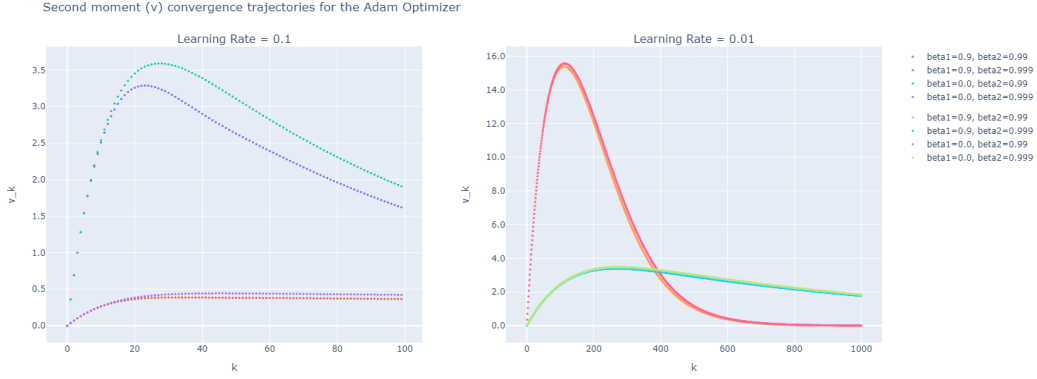


Figure 7: **Trajectory of the Second Moment for Adam Algorithm.** The convergence trajectories of the second moment  $v_k$  under different configurations of  $\beta_1$ ,  $\beta_2$ , and  $\alpha$ . Higher values of  $\beta_1$  and  $\beta_2$  result in a more gradual increase and smoother stabilization of  $v_k$ , while lower values lead to sharper peaks and rapid decreases.

can be characterized by the following equation:

$$\dot{\theta}^i(t) = -\frac{\partial^i f(\theta)}{\sqrt{G(t, \theta) + \epsilon}}, \quad (3)$$

where  $\epsilon$  is a small real value (typically  $\sim 10^{-8}$ ), and the nonlocal term  $G(t, \theta)$  is defined as:

$$G(t, \theta) = \frac{1}{\alpha} \int_0^t d\tau \partial^i f(\theta(\tau)) \partial_i f(\theta(\tau)).$$

*Proof.* Appendix A. □

This proposition highlights that the continuous-time model for AdaGrad is described by a first-order integro-differential equation. Notice that the nonlocality is embedded in the accumulated gradient term, where the entire trajectory of  $\theta$  up to time  $t$  must be known, along with a small differential time step (future) described by  $\alpha$ .

Now, we introduce the continuous model for RMSProp. Hence,

**Proposition 2 (Nonlocal Continuous Dynamics of RMSProp).** *Under Assumption (2) and given an initial value for the squared gradient moving average  $v_0 = 0$ , the continuous nonlocal dynamics of RMSProp can be characterized by the following equation:*

$$\dot{\theta}^i(t) = -\frac{\partial^i f(\theta)}{\sqrt{v(t, \theta) + \epsilon}}, \quad (4)$$

where  $\epsilon$  is a small real value (typically  $\sim 10^{-8}$ ), and the nonlocal term  $v(t, \theta)$  is defined as:

$$v(t, \theta) = \frac{1 - \beta}{\alpha} \int_0^t d\tau e^{-\frac{1-\beta}{\alpha}(t-\tau)} \partial^i f(\theta(\tau)) \partial_i f(\theta(\tau)).$$

*Proof.* Appendix A. □

As discussed earlier, a similar situation arises with RMSProp: the dynamics are governed by the integro-differential equation (4). The nonlocal behavior is encapsulated within the squared gradient moving average. It is necessary to know the value of  $\theta$  up to time  $t$  and a small time increment determined by  $\alpha$ .

The key difference between RMSProp and AdaGrad lies in the kernel of the integral operator. For AdaGrad, the kernel is

$$K_{AG}(t) = \frac{1}{\alpha}.$$

However, for RMSProp, the kernel is modified to:

$$K_{RP}(t) = \frac{1-\beta}{\alpha} e^{-\frac{1-\beta}{\alpha}t}.$$

This modification aligns with the behavior observed in Figure 4, where an exponential decay is evident as time (or iterations, in this context) progresses.

Finally, we introduce the continuous model for Adam:

**Proposition 3 (Nonlocal Continuous Dynamics of Adam).** *Under Assumption (2) and with initial values for the moments  $m_0^i = 0$  and  $v_0 = 0$ , the Adam optimizer can be characterized by the following continuous nonlocal dynamics:*

$$\dot{\theta}^i(t) = -\alpha(t) \frac{m^i(t, \theta)}{\sqrt{v(t, \theta) + \epsilon(t)}}, \quad (5)$$

where

$$\alpha(t) = \frac{\sqrt{1 - \beta_2^{\frac{t}{\alpha}}}}{1 - \beta_1^{\frac{t}{\alpha}}}, \quad \text{and} \quad \epsilon(t) = \epsilon \sqrt{1 - \beta_2^{\frac{t}{\alpha}}}, \quad (6)$$

and the moments are given by:

$$m^i(t, \theta) = \int_0^t d\tau K_1(t-\tau) \partial^i f(\theta(\tau)), \quad \text{and} \quad v(t, \theta) = \int_0^t d\tau K_2(t-\tau) \partial^i f(\theta(\tau)) \partial_i f(\theta(\tau)),$$

with the kernel function  $K_a(t)$  defined as:

$$K_a(t) = \frac{1 - \beta_a}{\alpha} e^{-\frac{1-\beta_a}{\alpha}t}, \quad a = 1, 2.$$

*Proof.* Appendix A. □

In the case of Adam, the nonlocality is encapsulated within both moments, as expected. A key distinction between Adam and other optimizers like AdaGrad or RMSProp (beyond the use of the exponential decay rates,  $\beta_1$  and  $\beta_2$ , and the specific kernel structure in AdaGrad) is that Adam does not require incorporating the future time differential  $\alpha$  that was necessary in the other cases.

These propositions confirm that the accumulative effects present in adaptive algorithms such as AdaGrad, RMSProp, and Adam are represented in continuous form as integro-differential equations (or nonlocal equations), where the presence of the kernel in the integral operator regulates the influence of the gradient on the dynamics.

Extensions to modifications of these algorithms, such as AdamW or AdamL2, can be derived similarly by adding:

- For AdamW:

$$\theta_t^i \leftarrow (1-w)\theta_{t-1}^i - \alpha \frac{\hat{m}_t^i}{\sqrt{\hat{v}_t + \epsilon}}.$$

- For AdamL2:

$$\partial^i f'_t(\theta_{t-1}) \leftarrow \delta^{ij} \partial_j f_t(\theta_{t-1}) + \frac{\lambda}{2} \theta_{t-1}^i$$

by following the same procedure used in the proof of Proposition (3). Here,  $\lambda$  denotes the regularization parameter, and  $w$  represents the weight decay parameter.

---

## 4 NUMERICAL SIMULATIONS

In this section, we present numerical simulations<sup>3</sup> that validate the approximations proposed in the preceding sections. As shown, the simulations closely mirror the behavior of the discrete algorithms, confirming that the first-order integro-differential equations serve as accurate and reliable models for analyzing the dynamics of these optimization methods. Additional numerical simulations related to the Mean Squared Error (MSE) loss function are provided in Appendix B. These further demonstrate, with an alternative example, how continuous models can effectively capture the dynamics of these optimization algorithms. Specifically, we simulate the convergence of the loss function while approximating the target function  $\hat{y}(x) = 2x$  using the model function  $y(x) = \theta x$ .

Before presenting the results, we provide an overview of the numerical method employed to solve the first-order integro-differential equations.

### 4.1 NUMERICAL METHOD

To solve these equations, we employed the IDESolver method as described in Gelmi & Jorquera (2014), which we implemented from scratch, tailoring the method to fit our specific requirements rather than using the existing Python module. See the pseudocode in Algorithm 4.

The numerical method operates as follows: It generates an initial guess for  $y(x)$  by disregarding the integral term (nonlocal part) in the equation and solving the resulting ordinary differential equation. This initial guess is then used to solve the original equation, and the new solution is compared to the initial guess. The similarity between the two is quantified by an error, defined as the sum of squared differences at the discretization points:

$$\text{error} = \sum_{n=1}^M (y_{\text{current},n} - y_{\text{guess},n})^2,$$

where  $M$  denotes the total number of discretization points,  $y_{\text{current},n}$  represents the current estimate of  $y$ , and  $y_{\text{guess},n}$  is the guess, both evaluated at the  $n$ -th step.

If the error exceeds a predefined tolerance, a new guess  $y_{\text{new}}$  is generated by a linear combination of the current  $y_{\text{current}}$  and the old guess  $y_{\text{guess}}$ :

$$y_{\text{new}} = ay_{\text{current}} + (1 - a)y_{\text{guess}}.$$

In our implementation, the value of  $a$  is adaptive, varying based on the error between iterations, and ranges from 0.5 to 0.9999. If the error increases between iterations,  $a$  is incremented by 0.0005. This adaptation allows for finer control of convergence. We set a global error tolerance of  $1 \times 10^{-4}$  and a maximum number of iterations of  $1 \times 10^{10}$ .

For the integral calculations, we employed Gaussian quadrature (`fixed_quad`) from SciPy with  $n = 1000$ , in place of the `quad` method used in the original paper. This leads to a significant increase in calculation speed. For the Adam optimizer, we further enhanced computational efficiency by parallelizing the integral computations.

Additionally, we used the Euler method to solve the differential equation, rather than the RK45 method commonly employed in the original approach, to ensure consistency with Assumption (2). The (future) time increment term  $\alpha$  of Propositions (1) and (2) is obtained using the `interp1d` interpolation function from SciPy.

This process continues until the error falls below the predefined tolerance. For further details on the implementation, please refer to the GitHub repository.

---

<sup>3</sup>All simulations can be reproduced from the repository available at GitHub.

---

**Algorithm 4** Iterative Modified IDESolver Method

---

```
1: Initialize the iteration counter  $k \leftarrow 0$ 
2: Compute the initial solution  $y_{\text{current}}$  using the original differential equation
3: Compute the initial guess  $y_{\text{guess}}$  including the integral part with  $y_{\text{current}}$ 
4: Calculate the initial global error  $\text{error} \leftarrow \|y_{\text{current}} - y_{\text{guess}}\|$ 
5: while  $\text{error} > \text{tolerance}$  do
6:   Compute new solution  $y_{\text{new}}$  using a smoothing factor with  $y_{\text{current}}$  and  $y_{\text{guess}}$ 
7:   Update  $y_{\text{guess}}$  solving the ODE including the integral part with  $y_{\text{new}}$ 
8:   Calculate the current global error  $\text{new\_error} \leftarrow \|y_{\text{new}} - y_{\text{guess}}\|$ 
9:   if  $\text{new\_error} > \text{error}$  then
10:    if maximum smoothing factor reached then
11:      Exit the loop without achieving the desired tolerance
12:    else
13:      Update the smoothing factor to the next value
14:    end if
15:  end if
16:  Update  $y_{\text{current}} \leftarrow y_{\text{new}}$ 
17:  Increment the iteration counter  $k \leftarrow k + 1$ 
18:  if  $k > k_{\text{max}}$  then
19:    Exit the loop
20:  end if
21:  Update  $\text{error} \leftarrow \text{new\_error}$ 
22: end while
23: Set the final solution  $y \leftarrow y_{\text{guess}}$ 
24: return time values and the corresponding solution  $y$ 
```

---

## 4.2 NUMERICAL RESULTS

In this section, we present the numerical results obtained using the numerical method described previously and compare them with the outcomes derived from the original algorithms.

It is important to clarify that throughout this section, when we refer to “iterations,” we specifically mean the value of  $k$  as defined by the relation:  $k = t/\alpha$ . This should not be confused with the iterations of the numerical method used to compute the solution. The latter refers to the internal steps required to obtain the overall solution, rather than the temporal evolution of  $\theta$ . To prevent confusion, we will use the term “k-iterations.”

**Nonlocal AdaGrad:** Figure 8 shows the convergence of  $\theta$  values using the nonlocal continuous AdaGrad method for minimizing the function  $(x - 4)^2$ , evaluated at two learning rates: 0.1 and 0.01. This figure demonstrates that the nonlocal continuous AdaGrad method effectively replicates the optimization dynamics of the conventional AdaGrad method.

Figure 9 depicts the evolution of the accumulated gradients  $G(t)$  under the nonlocal continuous AdaGrad method. For a learning rate of 0.1, the method converges to the target value  $\theta = 4$ , with  $G(t)$  stabilizing around 1,000 k-iterations. While this behavior closely matches the results observed with the conventional AdaGrad, a slight difference can be noted: the nonlocal continuous method reaches saturation slightly earlier than the discrete version.

When the learning rate is reduced to 0.01, the nonlocal continuous AdaGrad method still converges toward  $\theta = 4$ , with  $G(t)$  reaching slightly above 100,000 k-iterations. As shown in Figure 9, as the learning rate decreases, the nonlocal continuous method and the discrete AdaGrad model become nearly identical, both requiring approximately 150,000 k-iterations to achieve overall stabilization.

**Nonlocal RMSProp:** Figure 10 presents the convergence trajectories for  $\theta$  values using the first-order nonlocal continuous RMSProp optimizer. The figure includes two subplots corresponding to different learning rates (0.1 on the left and 0.01 on the right) and varying  $\beta$  parameters (0.0, 0.9, 0.99).



Figure 8: **Convergence of  $\theta(t)$  using the first-order nonlocal continuous AdaGrad method.** The plot illustrates the convergence trajectories for minimizing the function  $(x - 4)^2$  using two different learning rates: 0.1 (left) and 0.01 (right). At a higher learning rate (0.1), the algorithm rapidly converges to the target value  $\theta = 4$ , stabilizing in under 1,500 k-iterations. With a lower learning rate (0.01), the convergence is more gradual, reaching the target around 100,000 k-iterations. To clearly demonstrate how accurately the nonlocal continuous model reproduces the discrete dynamics, the plot also includes the simulation of the discrete AdaGrad, making it easier to observe their alignment.

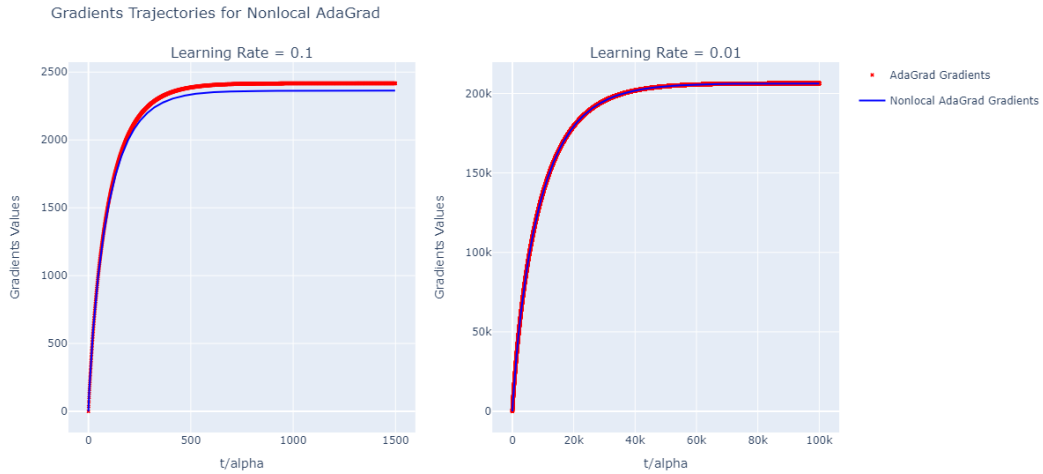


Figure 9: **Accumulated gradients  $G(t)$  convergence trajectories using the first-order nonlocal continuous AdaGrad method.** The plot shows that the nonlocal continuous AdaGrad method exhibits a nearly identical gradient accumulation behavior to the conventional AdaGrad method, with rapid convergence and stabilization at both learning rates.

For  $\theta$ , with a learning rate of 0.1,  $\beta = 0.99$  leads to faster convergence, while  $\beta = 0.9$  and  $\beta = 0.0$  result in slower convergence, with the latter exhibiting more linear behavior but showing noticeable oscillations. When the learning rate is reduced to 0.01, the overall convergence slows, and the oscillatory behavior for  $\beta = 0.0$  becomes less pronounced<sup>4</sup>.

<sup>4</sup>A slight oscillation is observed for  $\beta = 0.9$  and a learning rate of 0.01, induced by the numerical method, as the convergence error does not decrease below  $1 \times 10^{-4}$ .

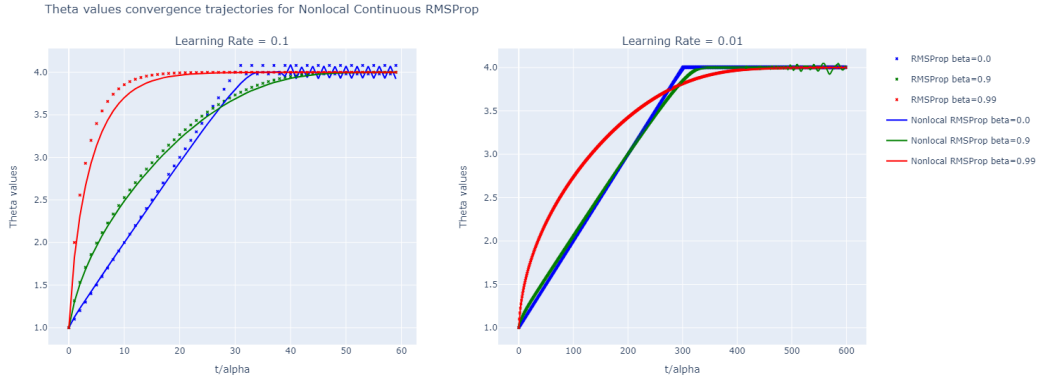


Figure 10: **Convergence of  $\theta(t)$  using the first-order nonlocal continuous RMSProp method.** The plot shows the convergence to the minimum value of  $\theta = 4$  for the function  $(\theta - 4)^2$ . The left subplot corresponds to a learning rate of 0.1, while the right subplot uses a learning rate of 0.01. With a learning rate of 0.1,  $\beta = 0.0$  exhibits more noticeable oscillations, whereas  $\beta = 0.9$  and 0.99 converge more smoothly. For a learning rate of 0.01, a slight destabilization occurs for  $\beta = 0.9$  as the solution approaches the final result, caused by the numerical method. We have also included the discrete RMSProp simulation to facilitate comparison. At higher learning rates, slight differences are observed: for  $\beta = 0.0$ , the oscillations in the discrete case start immediately upon reaching the minimum, whereas in the continuous case, they take a few k-iterations to begin. On the other hand, for  $\beta = 0.99$ , the curve is more pronounced in the discrete model compared to the continuous one.

Figure 11 shows the behavior of the squared gradients  $v(t)$  under the nonlocal continuous RMSProp method. With a learning rate of 0.1, lower  $\beta$  values initially produce a bump followed by a decay, while higher  $\beta$  values exhibit a less pronounced bump. When the learning rate is decreased, this bump becomes more noticeable.

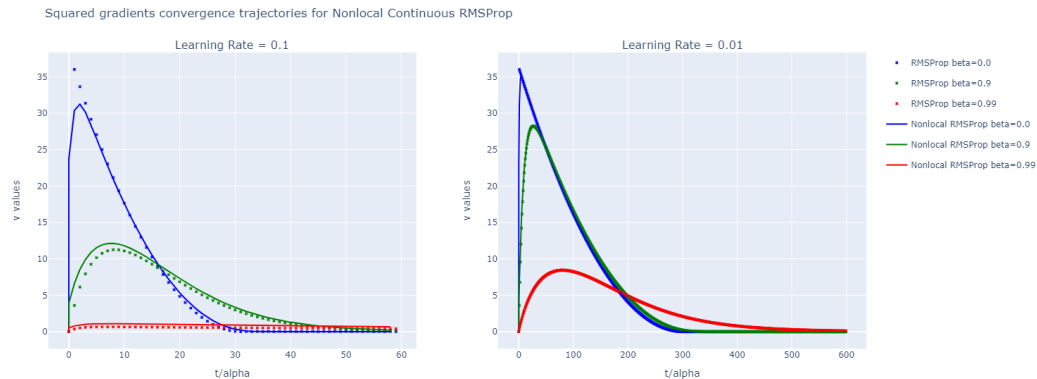


Figure 11: **Convergence trajectories of  $v(t)$  for the first-order nonlocal continuous RMSProp optimizer.** This plot illustrates the convergence of the squared gradient moving average  $v(t)$ . The left subplot represents a learning rate of 0.1, while the right subplot corresponds to a learning rate of 0.01. For  $\beta$  values of 0.0 and 0.9, a slight initial bump is noticeable, but both eventually decay towards zero. To enable a direct comparison, we have also included the discrete RMSProp case, demonstrating the strong alignment between the nonlocal continuous model and its discrete counterpart. The main differences appear with a learning rate of 0.1, where the values are slightly higher for  $\beta = 0.9$  and  $\beta = 0.99$ , and for  $\beta = 0.0$ , there is a slight bump rather than a direct descent.

When compared to the standard RMSProp optimizer, the nonlocal continuous variant exhibits a similar overall convergence pattern but with subtle differences. In the  $\theta$ -plot for a learning rate of

0.1 and  $\beta = 0.0$ , stability is achieved, but oscillations begin after a few iterations, in contrast to the conventional case where oscillations start immediately. Additionally, in the squared gradients plot, for  $\beta = 0.0$ , the continuous case initially shows a slight bump before gradually decaying, whereas in the discrete case, the decay occurs immediately without any “initial” increase. This difference arises because the continuous simulation captures a smoother temporal progression, while the discrete method reflects a more abrupt change.

Furthermore, for  $\beta = 0.9$  and  $\beta = 0.99$ , the nonlocal continuous model displays a slightly different dynamic compared to the discrete case, reaching slightly higher values. However, as the learning rate decreases, these differences diminish, and the models become almost identical, showcasing a near-perfect accuracy in the continuous representation.

**Nonlocal Adam:** Figures 12, 13, and 14 illustrate the behavior of the first-order nonlocal continuous Adam optimization model by showing the convergence trajectories of  $\theta(t)$ ,  $m(t)$ , and  $v(t)$  over time for different parameter settings ( $\beta_1$  and  $\beta_2$ ) and learning rates ( $\alpha = 0.1$  and  $\alpha = 0.01$ ).

Figure 12 shows the convergence of  $\theta$ . For a higher learning rate ( $\alpha = 0.1$ ), convergence is rapid, with different combinations of  $\beta_1$  and  $\beta_2$  reaching a stable value in fewer steps. However, for configurations with  $\beta_1 = 0.9$ , although convergence occurs more quickly, there are small oscillations, making the process slightly more unstable before reaching the minimum value. These oscillations are reduced when the learning rate is lowered to  $\alpha = 0.01$ . When the learning rate is lower, convergence is slower and more stable, with subtle differences in behavior between various parameter settings.

When compared to the discrete Adam model, the nonlocal continuous model is nearly identical at lower learning rates. However, for a learning rate of 0.1, slight differences can be observed: initially, for  $\beta_1 = 0.0$ , the continuous model diverges slightly, and for  $\beta_1 = 0.9$ , the peak is marginally higher than in the simulated discrete case. Nonetheless, these differences are minimal. As the learning rate decreases, both methods become almost exactly the same.

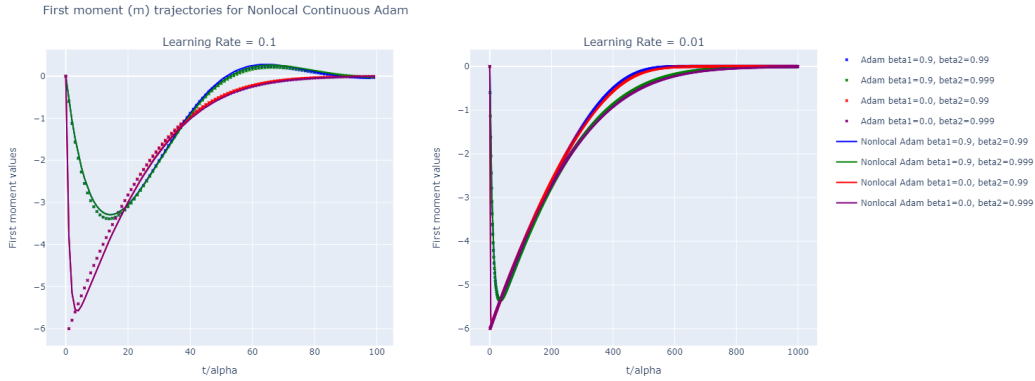


Figure 12: **Convergence of  $\theta(t)$  using the first-order nonlocal continuous Adam method.** The plot illustrates the convergence trajectories of  $\theta$ -values for the first-order nonlocal continuous Adam model under different parameter settings of  $\beta_1$  and  $\beta_2$  with two distinct learning rates (0.1 and 0.01). For  $\beta_1 = 0.9$  and a learning rate of 0.1, noticeable oscillations are observed, requiring a longer time to stabilize at the minimum value. This behavior improves when the learning rate is reduced to 0.01. Additionally, as expected, when the learning rate decreases, the number of k-iterations increases, indicating a slower convergence process. To highlight the high accuracy of the nonlocal continuous model compared to the discrete version, we have overlaid the discrete Adam simulations on the plot. This allows for a clear visualization of the remarkable similarity between both models.

Figure 13 highlights the evolution of the first moment  $m(t)$ . For a learning rate of  $\alpha = 0.1$ ,  $m(t)$  demonstrates a more pronounced oscillatory behavior before stabilizing around zero. When compared to the standard Adam optimizer’s convergence of the first moment  $m_k$ , both the nonlocal and standard Adam models show identical initial oscillatory patterns. With a reduced learning rate ( $\alpha = 0.01$ ), both models achieve smoother and more gradual convergence. The key difference is



that, regardless of the learning rate, the curve for  $\beta = 0.0$  begins more smoothly in the nonlocal model, while the standard model shows a more abrupt start.



**Figure 13: Convergence trajectories of  $m(t)$  for the first-order nonlocal continuous Adam optimizer.** The plot shows the evolution of the first moment  $m(t)$  over time, scaled by the learning rate. With a higher learning rate ( $\alpha = 0.1$ ), the values of  $m(t)$  exhibit certain oscillations, whereas a lower learning rate ( $\alpha = 0.01$ ) results in a smoother and slower convergence. To demonstrate the high level of accuracy of the nonlocal continuous model in replicating the discrete dynamics, the plot includes the discrete Adam simulations, allowing for a clear comparison between both approaches.

Figure 14 shows the evolution of the second moment  $v(t)$ . For a higher learning rate ( $\alpha = 0.1$ ), the nonlocal continuous Adam model displays varying peak values depending on the parameter settings. Configurations such as  $\beta_1 = 0.0$  and  $\beta_2 = 0.999$  produce the highest peaks and the slowest decay. When compared to the standard Adam optimizer's second moment  $v_k$ , both models follow similar trends, with distinct peak behaviors based on the parameter settings. Notably, the peaks for  $\beta_2 = 0.999$  are generally higher in the nonlocal model, whereas for  $\beta_2 = 0.99$ , the peaks are slightly lower.

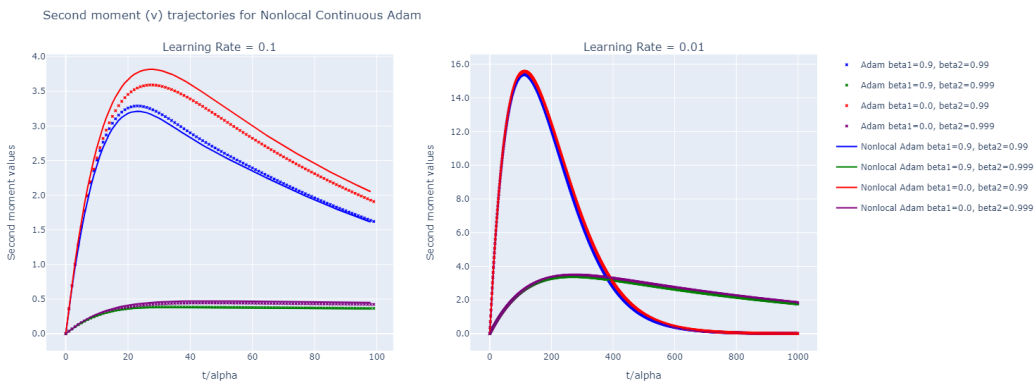


**Figure 14: Convergence trajectories of  $v(t)$  for the first-order nonlocal continuous Adam optimizer.** The plot illustrates the convergence of the squared gradient moving average  $v(t)$ . At a higher learning rate ( $\alpha = 0.1$ ), the peaks of  $v(t)$  vary according to the parameter settings, with  $\beta_1 = 0.0$  and  $\beta_2 = 0.999$  producing the most significant peak and the slowest rate of decay. When the learning rate is reduced to 0.01, all curves display a more pronounced initial peak followed by a gradual decline. To enhance the visual comparison and highlight the accuracy of the nonlocal continuous model, the plot also includes the results of the discrete Adam optimizer, allowing the reader to directly observe the close alignment between the two methods.

---

For a smaller learning rate ( $\alpha = 0.01$ ), the model shows an increase in the size of the peaks across all parameter settings, with a more pronounced bump for  $\beta_1 = 0.0$ , identical to the behavior observed in the standard case.

## 5 CONCLUSION

In this paper, we have introduced a continuous-time formulation for the AdaGrad, RMSProp, and Adam optimization algorithms by modeling them as first-order integro-differential equations. This novel approach captures the cumulative and memory effects inherent in these adaptive methods, providing a unified and precise mathematical framework that bridges the gap between discrete algorithms and continuous dynamical systems.

Our continuous models establish a direct connection between the discrete implementations of these algorithms and their continuous counterparts. The nonlocal integral terms naturally encapsulate the algorithms' memory and adaptive behaviors, allowing us to represent the influence of past gradients on current updates explicitly. Through extensive numerical simulations, we have demonstrated that these continuous formulations accurately replicate the convergence dynamics and behaviors of the original algorithms across various settings, including different learning rates and parameter configurations. Furthermore, as the learning rate is reduced, the similarity between the continuous and discrete models increases, further confirming the effectiveness of the continuous representation in capturing the behavior of the discrete algorithms.

However, while our continuous-time models provide valuable insights, they are based on deterministic settings and simplified objective functions. Extending these models to handle stochasticity, high-dimensional parameter spaces, and the complex architectures of modern neural networks is a natural next step. Furthermore, addressing the computational complexity associated with solving integro-differential equations is essential for enhancing their practical applicability, highlighting the need for efficient computational strategies.

In conclusion, our findings suggest that the integro-differential approach not only provides a valid method for representing the dynamics of AdaGrad, RMSProp, and Adam in a continuous-time framework but also serves as a powerful tool for advancing the theoretical understanding of these widely used optimization algorithms. By bridging discrete and continuous optimization methods, this approach has the potential to inspire novel methodologies and applications in AI research that involve memory (nonlocal) effects. Such applications include nonlocal Lagrangian or Hamiltonian formalisms and the extension of Noether's Theorem for nonlocal Lagrangians, which we could further explore in future work Heredia & Llosa (2021); Heredia (2023).

## ACKNOWLEDGMENTS

I would like to express sincere gratitude to Josep Llosa (University of Barcelona), Rhys Gould (University of Cambridge), Hidenori Tanaka (Harvard University), and Javier Cristin (Autonomous University of Barcelona) for their insightful discussions on nonlocality and valuable feedback on this manuscript. I also thank the Digital Transformation Team and the Nennisiwok Team at DAMM for their ongoing support.

## REFERENCES

- Ferran Alet, Dylan Doblar, Allan Zhou, Josh Tenenbaum, Kenji Kawaguchi, and Chelsea Finn. Noether networks: meta-learning useful conserved quantities. *Advances in Neural Information Processing Systems*, 34:16384–16397, 2021.
- Léon Bottou. Large-scale machine learning with stochastic gradient descent. In Yves Lechevallier and Gilbert Saporta (eds.), *Proceedings of COMPSTAT'2010*, pp. 177–186, Heidelberg, 2010. Physica-Verlag HD. ISBN 978-3-7908-2604-3.
- Stephen P Boyd and Lieven Vandenberghe. *Convex optimization*. Cambridge university press, 2004.
- Ricky TQ Chen, Yulia Rubanova, Jesse Bettencourt, and David K Duvenaud. Neural ordinary differential equations. *Advances in neural information processing systems*, 31, 2018.

- 
- Miles Cranmer, Sam Greydanus, Stephan Hoyer, Peter Battaglia, David Spergel, and Shirley Ho. Lagrangian neural networks. *arXiv preprint arXiv:2003.04630*, 2020.
- John Duchi, Elad Hazan, and Yoram Singer. Adaptive subgradient methods for online learning and stochastic optimization. *Journal of Machine Learning Research*, 12(61):2121–2159, 2011.
- Weinan E. A proposal on machine learning via dynamical systems. *Communications in Mathematics and Statistics*, 5(1):1–11, 2017. doi: 10.1007/s40304-017-0103-z.
- F.R. Gantmakher. *Lectures in Analytical Mechanics: Translated from the Russian by George Yankovsky*. Mir Publishers, 1970.
- Claudio A. Gelmi and Héctor Jorquera. Idsolver: A general purpose solver for nth-order integro-differential equations. *Computer Physics Communications*, 185(1):392–397, 2014. ISSN 0010-4655. doi: doi.org/10.1016/j.cpc.2013.09.008.
- Samuel Greydanus, Misko Dzamba, and Jason Yosinski. Hamiltonian neural networks. *Advances in neural information processing systems*, 32, 2019.
- Carlos Heredia. Nonlocal lagrangian formalism, 2023.
- Carlos Heredia and Josep Llosa. Non-local lagrangian mechanics: Noether’s theorem and hamiltonian formalism. *Journal of Physics A: Mathematical and Theoretical*, 54(42):425202, September 2021. ISSN 1751-8121. doi: 10.1088/1751-8121/ac265c.
- Geoffrey Hinton. Lecture 6: Training a multilayer neural network. University of Toronto, 2012. CSC321: Neural Networks for Machine Learning.
- H. K. Khalil. *Nonlinear Systems*. Prentice Hall, Upper Saddle River, NJ, 3rd edition, 2002.
- Diederik P Kingma and Jimmy Ba. Adam: A method for stochastic optimization. *arXiv preprint arXiv:1412.6980*, 2014.
- Nikola B Kovachki and Andrew M Stuart. Continuous time analysis of momentum methods. *Journal of Machine Learning Research*, 22(17):1–40, 2021.
- Qianxiao Li, Cheng Tai, and Weinan E. Stochastic modified equations and adaptive stochastic gradient algorithms. In Doina Precup and Yee Whye Teh (eds.), *Proceedings of the 34th International Conference on Machine Learning*, volume 70 of *Proceedings of Machine Learning Research*, pp. 2101–2110. PMLR, 06–11 Aug 2017.
- Ilya Loshchilov and Frank Hutter. Decoupled weight decay regularization. *arXiv preprint arXiv:1711.05101*, 2017.
- Orlando Romero, Mouhacine Benosman, and George J. Pappas. Ode discretization schemes as optimization algorithms. In *2022 IEEE 61st Conference on Decision and Control (CDC)*, pp. 6318–6325, 2022. doi: 10.1109/CDC51059.2022.9992691.
- Sebastian Ruder. An overview of gradient descent optimization algorithms. *arXiv preprint arXiv:1609.04747*, 2016.
- David E. Rumelhart, Geoffrey E. Hinton, and Ronald J. Williams. Learning internal representations by error propagation. 1986.
- Lars Ruthotto and Eldad Haber. Deep neural networks motivated by partial differential equations. *Journal of Mathematical Imaging and Vision*, 62(3):352–364, 2020. doi: 10.1007/s10851-019-00903-1.
- Justin Sirignano and Konstantinos Spiliopoulos. Stochastic gradient descent in continuous time. *SIAM Journal on Financial Mathematics*, 8(1):933–961, 2017.
- Weijie Su, Stephen Boyd, and Emmanuel J. Candès. A differential equation for modeling nesterov’s accelerated gradient method: Theory and insights. *Journal of Machine Learning Research*, 17(153):1–43, 2016.

Hidenori Tanaka and Daniel Kunin. Noether’s learning dynamics: Role of symmetry breaking in neural networks. *Advances in Neural Information Processing Systems*, 34:25646–25660, 2021.

Andre Wibisono, Ashia C Wilson, and Michael I Jordan. A variational perspective on accelerated methods in optimization. *proceedings of the National Academy of Sciences*, 113(47):E7351–E7358, 2016.

Emanuele Zappala, Antonio Henrique de Oliveira Fonseca, Andrew Henry Moberly, Michael James Higley, Chadi Abdallah, Jessica Cardin, and David van Dijk. Neural integro-differential equations, 2022.

## APPENDIX

### A PROOFS

In this section, we present detailed proofs for Propositions 1 to 3.

#### Proof of Proposition 1:

*Proof.* To facilitate the proof, we begin by shifting the temporal indexing from  $k \leftarrow k + 1$  to  $k + 1 \leftarrow k$ . Consequently, the parameter update rule becomes:

$$\theta_{k+1}^i = \theta_k^i - \alpha \frac{\partial^i f(\theta_k)}{\sqrt{G_{k+1} + \epsilon}}.$$

By applying Assumption (2), the evolution of the accumulated gradients can be described by the differential equation:

$$\dot{G}(t, \theta) = \frac{1}{\alpha} \partial^i f(\theta) \partial_i f(\theta),$$

whose solution (for  $t > 0$ ) is:

$$G(t, \theta) = \frac{1}{\alpha} \int_0^t d\tau \partial^i f(\theta(\tau)) \partial_i f(\theta(\tau)).$$

Using Assumption (2) again, we derive the integro-differential equation that governs the updated parameters:

$$\dot{\theta}^i(t) = -\frac{\partial^i f(\theta)}{\sqrt{G(t + \alpha, \theta) + \epsilon}}.$$

□

#### Proof of Proposition 2:

*Proof.* To simplify the proof, as in Proposition 1, we shift the indexing such that  $k + 1 \leftarrow k$ . The parameter update then becomes:

$$\theta_{k+1}^i = \theta_k^i - \alpha \frac{\partial^i f(\theta_k)}{\sqrt{v_{k+1} + \epsilon}}.$$

By applying Assumption (2), the evolution of the squared gradient moving average is governed by the differential equation:

$$\dot{v} + \frac{1 - \beta_2}{\alpha} v = \frac{1 - \beta_2}{\alpha} \partial^i f(\theta) \partial_i f(\theta). \quad (7)$$

Rewriting this equation yields:

$$\frac{d}{dt} \left[ e^{\frac{1-\beta_2}{\alpha} t} v \right] = \frac{1 - \beta_2}{\alpha} e^{\frac{1-\beta_2}{\alpha} t} \partial^i f(\theta) \partial_i f(\theta), \quad (8)$$

which leads to the solution (for  $t > 0$ ):

$$v(t, \theta) = \frac{1 - \beta_2}{\alpha} \int_0^t d\tau e^{-\frac{1-\beta_2}{\alpha}(t-\tau)} \partial^i f(\theta(\tau)) \partial_i f(\theta(\tau)). \quad (9)$$

Finally, by applying Assumption (2), the parameter updates follow the integro-differential equation:

$$\dot{\theta}^i(t) = -\frac{\partial^i f(\theta)}{\sqrt{v(t+\alpha, \theta)} + \epsilon}. \quad (10)$$

□

### Proof of Proposition 3:

*Proof.* To prove this proposition, we start from step 5-6 of Algorithm 3:  $m_k^i = \beta_1 m_{k-1}^i + (1-\beta_1)g_k^i$  and  $v_k = \beta_2 v_{k-1} + (1-\beta_2)g_k^2$ . Since the structure is identical for both moments, we demonstrate the process for one, knowing the other will follow similarly, except for differences in the exponential decay or gradient. We redefine the indices as  $k+1 \leftarrow k$  to avoid involving  $\theta_{t-1}$  in the gradient.

Focusing on the second moment  $v$ , we use the same approach as in Proposition 2 to obtain:

$$v(t, \theta) = \frac{1-\beta_2}{\alpha} \int_0^t d\tau e^{-\frac{1-\beta_2}{\alpha}(t-\tau)} \partial^i f(\theta(\tau)) \partial_i f(\theta(\tau)). \quad (11)$$

The first moment  $m^i(t, \theta)$  follows a similar pattern, differing by the absence of the squared gradient and the exponential decay factor  $\beta_2$ :

$$m^i(t, \theta) = \frac{1-\beta_1}{\alpha} \int_0^t d\tau e^{-\frac{1-\beta_1}{\alpha}(t-\tau)} \partial^i f(\theta(\tau)). \quad (12)$$

Applying Assumptions (2) and (1) and performing some algebraic manipulations yields:

$$\dot{\theta}^i(t) = -\alpha(t) \frac{m^i(t, \theta)}{\sqrt{v(t, \theta)} + \epsilon(t)}, \quad (13)$$

where

$$\alpha(t) = \frac{\sqrt{1-\beta_2^{\frac{t}{\alpha}}}}{1-\beta_1^{\frac{t}{\alpha}}}, \quad \text{and} \quad \epsilon(t) = \epsilon \sqrt{1-\beta_2^{\frac{t}{\alpha}}}. \quad (14)$$

□

## B ADDITIONAL NUMERICAL SIMULATIONS

In this appendix, we present additional simulations for the nonlocal continuous models and compare them with their conventional counterparts. Unlike the simulations presented in Section 4.2, this section focuses on the convergence behavior of the Mean Squared Error (MSE) loss function for the function  $y(x) = 2x$ , where the target parameter value to be obtained is 2.

The settings for these simulations were as follows:

- **Figure 15:** Simulations were performed with RMSProp ( $\beta = 0.9$ ) and Adam ( $\beta_1 = 0.9, \beta_2 = 0.99$ ) optimizers, using learning rates of 0.1 and 0.01, respectively. The parameter  $\theta_0$  was initialized to 0. To ensure computational efficiency, simulations were limited to 60 k-iterations for a learning rate of 0.1 and 300 k-iterations for a learning rate of 0.01, which was sufficient to capture the desired behavior.
- **Figure 16:** Simulations were conducted with RMSProp ( $\beta = 0.99$ ) and Adam ( $\beta_1 = 0.99, \beta_2 = 0.999$ ) optimizers, again using learning rates of 0.1 and 0.01, respectively. The parameter  $\theta_0$  was initialized to 0. To maintain computational efficiency, simulations were capped at 80 k-iterations for a learning rate of 0.1 and 500 k-iterations for a learning rate of 0.01.

Figures 15 and 16 demonstrate that the numerical simulations of the integro-differential equations closely match the results of the discrete models, regardless of the optimizer used, reaffirming the validity of the continuous models. As expected, the AdaGrad model is more computationally intensive to reach a loss of 0, while RMSProp achieves convergence more quickly. An interesting observation is that, for a learning rate of 0.1, the nonlocal models accurately reproduce the bump around 35 k-iterations, which gradually diminishes as the learning rate decreases. Moreover, it is evident that as the learning rate is lowered, the continuous model more closely approximates the behavior of the discrete model.

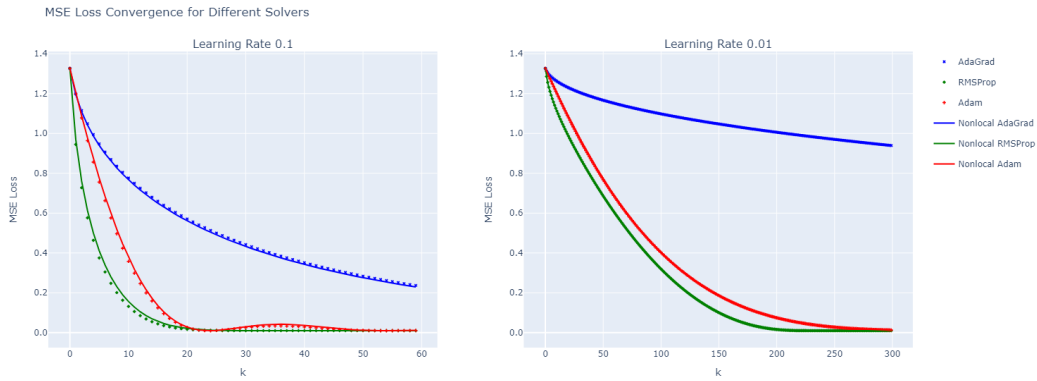


Figure 15: **MSE Loss Convergence for Different Solvers.** The plots show the convergence behavior of the Mean Squared Error (MSE) loss for various optimization algorithms (AdaGrad, Adam, and RMSProp) along with their nonlocal continuous versions, evaluated at two different learning rates (0.1 and 0.01). The left plot shows results for a learning rate of 0.1, while the right plot presents those for a learning rate of 0.01. The configurations used are RMSProp with  $\beta = 0.9$  and Adam with  $\beta_1 = 0.9$  and  $\beta_2 = 0.99$ . In general, lower learning rates tend to produce smoother convergence curves, whereas higher learning rates can accelerate initial convergence but often lead to more fluctuations.

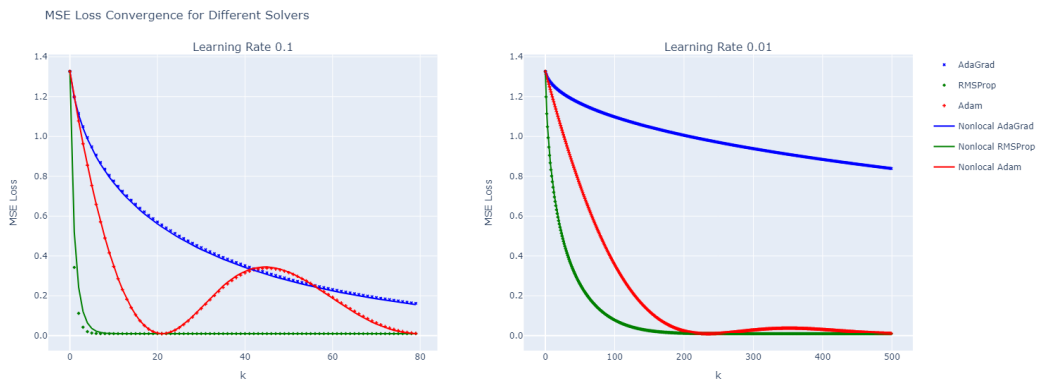


Figure 16: **MSE Loss Convergence for Different Configuration Solvers.** The plots display the convergence of the Mean Squared Error (MSE) loss for various optimization algorithms (AdaGrad, Adam, and RMSProp) and their nonlocal continuous counterparts, using two different learning rates (0.1 and 0.01). The configurations include RMSProp with  $\beta = 0.99$  and Adam with  $\beta_1 = 0.99$  and  $\beta_2 = 0.999$ . Lower learning rates typically produce smoother convergence curves, whereas higher learning rates may lead to faster initial convergence but can also cause more pronounced fluctuations.